RESEARCH ARTICLE

Low-Cost Direct-Writing of Silver-Based Ink for Planar Microwave Circuits up to 10 GHz

CAROLINA BLANCO-ANGULO[1], **ANDREA MARTÍNEZ-LOZANO**[1],
JULIA ARIAS-RODRÍGUEZ[1], **ALBERTO RODRÍGUEZ-MARTÍNEZ**[2], **(Senior Member, IEEE)**,
JOSÉ MARÍA VICENTE-SAMPER[3], **JOSÉ MARÍA SABATER-NAVARRO**[3], **(Senior Member, IEEE)**,
AND ERNESTO ÁVILA-NAVARRO[1]

[1]Department of Materials Science, Optics and Electronic Technology, Miguel Hernández University of Elche, 03202 Elche, Spain
[2]Communication Engineering Department, Miguel Hernández University of Elche, 03202 Elche, Spain
[3]Neuroengineering Biomedical Research Group, Miguel Hernández University of Elche, 03202 Elche, Spain

Corresponding author: Julia Arias-Rodríguez (julia.arias@umh.es)

ABSTRACT Direct ink writing (DIW) of conductive ink is a printed electronics technology that allows a variety of electronic circuits to be produced in a simple way and with minimal waste of materials. In recent years it has been used for rapid prototyping of RF circuits typically working at S-band frequencies (2–4 GHz). In an attempt to extend this frequency range while maintaining cost-effective prototyping, this work has focused on proving the feasibility of DIW of silver-conductive (SC) ink for the fabrication of planar microwave circuits beyond 10 GHz, more specifically, ultra-wideband (UWB) antennas for medical applications. For this purpose, the DC and RF performance of the SC ink, as well as the FR4 substrate used, were first evaluated. Based on the comparison between experimental and simulated results, we have found that the effective RF conductivity of the SC ink is approximately 27.6% of its DC value and 3.4% of the copper conductivity. A few test microstrip circuits were fabricated by DIW, namely two S-band filters and one UWB antenna. The overall measured performance of all of them agreed well with simulations. In particular, the DIW antenna exhibited a bandwidth of 8.2 GHz (between 2.4 and 10.6 GHz), and was compared with an identical copper antenna showing that both have very similar characteristics. It was also found that the lower conductivity of SC ink as compared to copper led to a gain reduction of only 0.3 dB.

INDEX TERMS Direct-ink-writing, silver-conductive ink, additive manufacturing, printed electronics, ultra-wideband antennas, electrical conductivity, conductor losses, ultrasonic non-destructive testing.

I. INTRODUCTION

Additive manufacturing (AM) and printed electronics (PE) bring together a series of emerging technologies that have been developed in recent years, providing solutions in a wide variety of fields such as medicine, construction, communications, energy harvesting, consumer electronics, etc. [1], [2], [3]. In this scenario, effort is being invested in manufacturing complex objects with unique features but also in taking advantage of the low manufacturing cost offered by some

The associate editor coordinating the review of this manuscript and approving it for publication was Qi Luo.

of these rapid prototyping systems [4], [5], [6]. PE offers attractive manufacturing cost-effectiveness due to its intrinsic characteristics such as affordability, adaptability to new substrates, low material waste, simplified processing, and high prototyping speed. PE has demonstrated outstanding versatility to work with a wide variety of flexible and non-flexible substrates, allowing the use of both organic [7] and inorganic materials and overcoming the limitation of using standard commercial wafers, as opposed to conventional wafer-based fabrication techniques. So far PE has been applied to manufacture printed sensors [8], [9], [10], [11], [12], [13], thin-film transistors [14], radio frequency identification tags (RFID)

[15], [16], energy harvesters [17], passive components [18], conformal electronics [19], etc. In particular, printed antennas are widely used as part of smart sensing systems [20] and PE techniques have further extended their use to numerous applications [21], [22], [23], [24], [25], [26]. More recently, effort is being invested in the development of non- invasive medical diagnostic techniques based on microwave imaging systems, with printed antennas as the primary sensing elements [27], [28], which offer a cost-effective and promising medical imaging solution but currently present some challenges for use in clinical settings [29].

Most printable materials are in the form of solutions, which need to have specific properties to enable proper printing. Conductive materials are the main structural blocks of all electronic devices, as they form the fundamental part of the device layers or interconnections. Among all possible candidates for printable conductive materials, silver conductive (SC) inks based on silver nanoparticles are the most widely used due to their high electrical conductivity and low oxidation rate. SC ink conductivity is usually enhanced by thermal sintering and the final conductivity value depends on several factors such as the nature of the ink (metal content, particle size and shape), sintering temperature and time [30], [31], [32], [33].

There are many printing options for additive electronics: inkjet, screen printing, direct-ink-writing (DIW) (also known as extrusion printing), flexographic, gravure, aerosol, etc. [3]. Unlike other PE techniques such as inkjet or screen printing, where a swath or an entire pattern is printed at once, DIW requires a nozzle to be moved relative to the substrate to draw and fill in the entire pre-programmed pattern feature-by-feature [34]. Basically, the nozzle moves like a pencil across the paper to leave the pattern on the substrate, one trace at a time. While feature-by-feature printing is inherently slower than high-throughput mass manufacturing methods, DIW excels in low volume prototyping and in applications with a high degree of customization, where other non-digital technologies such as screen-printing struggle [35], [36]. However, when it comes to microwave applications, this low-cost and easy-to-use technique has the disadvantage of a higher manufacturing tolerance and a lack of information on the behavior of conductive inks at high frequency. It is known that the effective conductivity can vary as a function of operating frequency. In this regard, there are several works on the performance of conductive inks used in direct-writing for RF applications up to 4 GHz [37], and 6 GHz [38]. This could explain why the RF applications in which conductive ink direct-write dispensing has been used do not go beyond 4.5 GHz [8], [24].

Within this context, this work is presented as a step-by-step study of the suitability of employing a SC ink DIW system for microwave applications beyond 10 GHz using an affordable DIW plotter, standard low-cost FR4 printed circuit boards (PCBs) and the experience of our research group in the design of ultra-wideband (UWB) antennas for medical imaging systems. One of the most important components of

a microwave-based medical imaging system is the antenna that is responsible for transmitting and receiving the electromagnetic energy used to generate the images. The useful frequency range for this type of application lies between 1 and 10 GHz, where both good wave penetration into tissue and spatial resolution can be achieved [39], [40], [41]. Antennas used in such systems must therefore cover this frequency band as well as possible and be sized appropriately for the application. This is the case for UWB antennas, as they have a relatively small size and cover a large part of the frequency range used in microwave medical imaging systems, which according to the standard should be in the range of 3.1 to 10.6 GHz.

The main objective of this work is, therefore, to provide a detailed methodology to properly characterize the design and fabrication process of planar microwave circuits with additive technology based on conductive inks, with the ultimate goal of extending the use of this low-cost dispensing technology to frequencies where it has not been applied so far. The versatility of this type of fabrication system in combination with the aforementioned methodology will allow cost-effective exploration of new UWB antenna topologies, but it will also enable printing on flexible substrates, which is particularly convenient when antennas need to be tailored to the contours of the human body.

After this introduction, this paper is organized as follows. Section II describes the DIW system and the materials used. In Section III, a thickness measurement technique using ultrasounds is applied in combination with the measurement of the DC electrical resistance to determine the DC conductivity of the deposited ink. RF methods for the characterization of the substrate used are also described in this section. Section IV presents the designed and fabricated prototypes and verifies their experimental performance by comparison with electromagnetic simulations, thus demonstrating the feasibility of the system and the materials being used. Finally, the main conclusions of this work are summarized in Section V.

II. MATERIALS AND MANUFACTURING PROCESS

The printer used in this work is the Voltera V-One PCB printer [42]. It is an easy-to-use multifunctional prototyping system that uses conductive ink or/and solder paste to print a circuit board design from Gerber files produced on any CAD tool and has a built-in reflow platform for subsequent ink curing or/and component soldering. The printer also has interchangeable drill heads for making variable width vias and thru-holes. The manufacturer specifies a minimum trace width of 0.2 mm and a minimum pin-to-pin pitch of 0.65 mm. Fig. 1(a) shows a picture of the Voltera V-One printing a PCB in the laboratory. The available area for print circuits is 135 mm × 114 mm.

This machine allows to print different types of conductive ink. In this work, a silver conductive (SC) ink from Voltera company has been used (Voltera Conductor 2, Ref. 1000388) [43]. According to manufacturer datasheet, some characteristics of this SC ink are: sheet resistance of 2.05 mΩ/sq
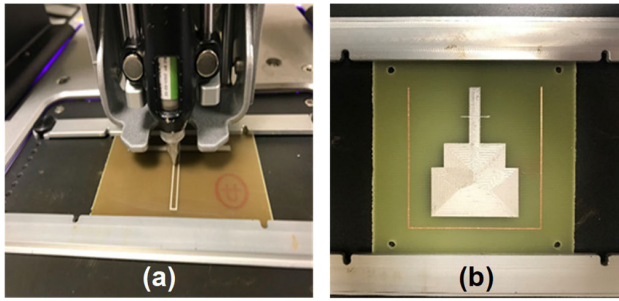
FIGURE 1. (a) The Voltera V-One device during the manufacture of a circuit. (b) Two-layer circuit manufacturing with reference marks.

for a 50 μm film thickness, resistivity (4-points probe) of 1.265×10^{-7} Ω·m, and density of 3.35 g/ml. The manufacturer guidelines state a curing temperature and time of 210 °C and 30 minutes, respectively. SC ink should be stored in the refrigerator when not used.

The substrate used for all circuits in this work is a 1.5 mm thick low cost FR4 type substrate, a composite of woven fiberglass cloth with an epoxy resin binder. Connectors were soldered by means of a low melting temperature solder paste alloy, Sn42/Bi57.6/Ag0.4.

The standard procedure for circuit fabrication consists of four steps. First, the board has to be correctly aligned in the printer and the printing area of the circuit has to be defined on the board. Next, the printer measures the height at different points of the printing area to compensate for possible irregularities on the board. This process is performed automatically by the printer software, generating a height map of the entire printing area. Once the circuit, the printing area and the height map are defined, a preliminary high precision calibration is performed to adjust the appropriate amount of ink to be deposited by the printer during the circuit drawing. Once calibrated, the printer can start printing the circuit. After a first print pass it is possible to perform another pass by changing the height of the printing nozzle, so that one pass deposits ink on top of the previous one without removing the existing material. Finally, when the circuit is completely drawn with the conductive ink, the ink is cured using the oven function of the printer by means of a hot plate. To facilitate the transfer of heat from the printing plate to the ink, the board is rotated to leave the circuit upside down.

In the case of having to manufacture two-layer circuits, it is necessary to apply two ink curing processes, since once the ink has been deposited on one side of the board, it will be necessary to cure it before applying the ink on the other side. In addition, it will be necessary to define a reference that allows the board to be correctly oriented and aligned for ink deposition on both sides. To do this, holes are drilled at different points on the board to align the circuit on both sides. Fig. 1(b) shows a two-layer circuit printed using this method. The four drills can be seen at the corners of the board, as well as a copper mark on the substrate. Once the printing

is complete, the board is trimmed, thus removing both the copper mark and the reference holes.

III. CHARACTERIZATION METHODS

Structural analysis, DC resistance measurements and microwave substrate characterization have been performed as a priori evaluation of the manufacturability of microwave circuits by SC ink dispensing.

A. STRUCTURAL ANALYSIS

A simple PCB trace geometry was selected to evaluate DC electrical conductivity of the SC ink. Ground plane was removed prior to ink deposition. The nominal length and width of the conductive trace were 50 and 3 mm, respectively, and were held constant throughout all sample configurations. Trace thickness was varied as a result of changing the number of print passes. In this way, three batches of samples of 2, 3 and 4 deposited layers were manufactured, each batch containing 5 nominally identical traces. For control and comparison purposes, an additional batch of copper traces with nominally identical length and width was realized on a photoresist FR4 substrate with copper cladding by UV exposure followed by development of exposed photoresist, and etching of unwanted conductive area.

Firstly, a structural analysis was performed on all the above traces in order to determine their thicknesses. Next, DC electrical resistance measurements were carried out. Results of both types of characterization were used to estimate SC ink conductivity.

The structural analysis is made using ultrasonic non-destructive testing techniques. The circuits were scanned in an immersion basin in distilled water, using a 5 MHz focused transducer V309 from OLYMPUS as pulse-echo transducer, with a focal diameter of around 0.5 mm. C-scans (2D scans along all the surface) were acquired for all specimens in the region of interest, taking measurements every 200 μm in X and Y axis. The ultrasonic system was from KTU Electronics, with a 10 bits DAC at 100 MSa/s. Fig. 2(a) shows the described set-up and Fig. 2(b) an example of one of the circuits under analysis, consisting on simple lines printed using respectively 2, 3 and 4 layers of SC ink on commercial FR4 boards, which will be compared with the same structure built using conventional copper chemical etching.

To calculate the thickness of the printed lines, conventional time-domain processing techniques were used to estimate the front-surface profile of each specimen. This is made calculating the Time-of-Flight (ToF) between each A-scan of the C-scan and a delayed reference A-scan, using the cross-correlation in frequency domain as describe in [5]. The reference echo was delayed artificially to ensure that all ToF have the same sign, which will ease the automatic thickness measurement. The thickness is obtained from the ToF using the propagation velocity of sound in distilled water (1498 m/s) at room temperature (25 °C), which was also measured and controlled during all the acquisition stage.
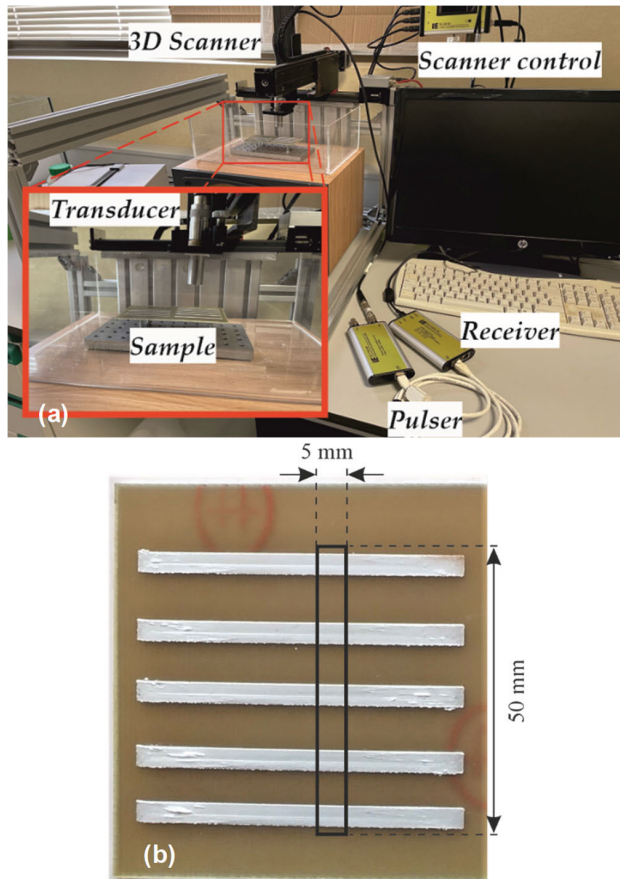
FIGURE 2. (a) Set-up of ultrasonic structural analysis experiment for the determination of ink layers. (b) Example of sample under analysis.

FIGURE 3. Thickness analysis for lines printed with four SC-ink layers. (a) 3D thickness profile. (b) Thickness profile at a particular cross-section. (c) Thickness distribution (probability density function, pdf).

First, the circuit shows a slight bending (note the difference between the straight dotted line and the interpolated red line, fitted with a parabolic interpolator), which cannot be corrected using the conventional calibration procedure embedded in the printer, resulting in a slight difference in thickness across the printing surface (see the ones at the outermost left and right in Fig. 3(b)). This board bending probably developed during the ink curing process due to the missing ground plane, and would not be present in microstrip circuits (which do have a ground plane). In any case, the observed bending value is rather small, only appreciable by the high resolution of the ultrasonic structural analysis and, were it present in RF circuits, it would hardly be reflected in their electromagnetic behavior. Note that the linear positive slope of the circuit (Fig. 3(a)) is due to mechanical misalignment between the circuit and the transducer, easily corrected by postprocessing for thickness estimation, and unconnected to the circuits manufacturing process. The board bending is also corrected in postprocessing using the same alignment algorithms, in order to calculate the actual thickness.

Second, there is also an evident difference across the profile of the printed line between the outer parts and the center, due to the printing procedure. This is because the lines are print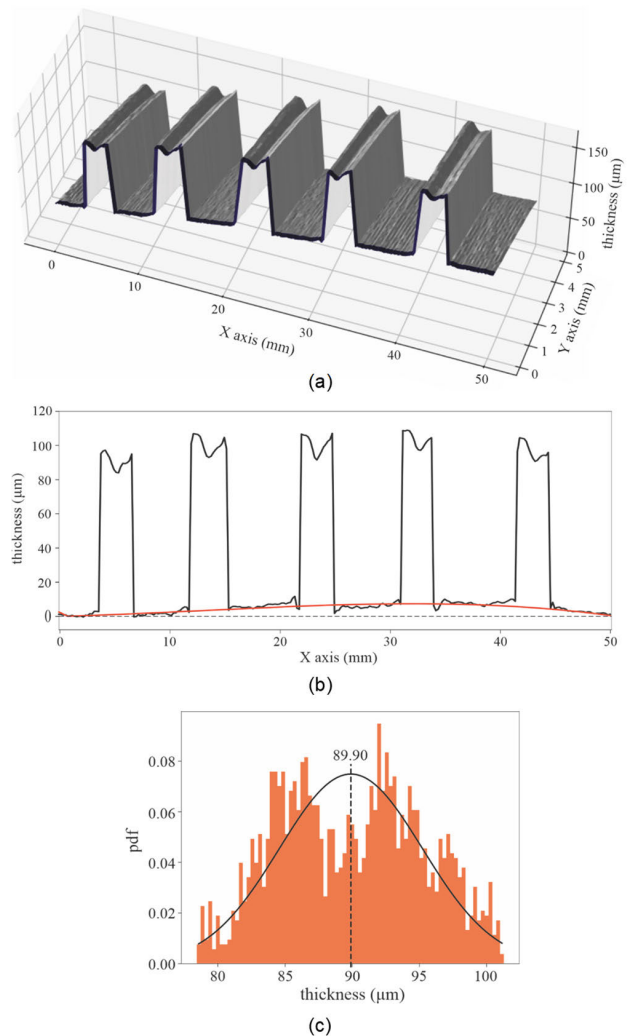ed using a spiraling rectangle pattern from the outside to the inside. Therefore, the last layers (the most center ones) will press the excess of ink towards the lateral sides of the extruder. The resulting thickness distribution (histogram) of the whole circuit after alignment is shown in Fig. 3(c), where the corresponding Gaussian distribution fitting is superimposed. Note that although the average thickness is 89.90 μm, there are two prevalence around 85 μm and 93.50 μm corresponding to the center and the outer layers respectively. This effect will be different depending on the width of the lines, the number of layers and the height between the extruder and the circuit, which will be also different among different parts of the circuits if it is slightly bended, which is the case of conventional commercial FR4 boards.

Fig. 4 shows the distributions (histograms) of the thickness for all the specimens under analysis with their corresponding Gaussian fitting and average thickness (black dotted lines), whose statistics are summarized in Table 1. As expected, the circuit built using conventional cooper chemical etching

TABLE 1. Measured thickness using ultrasounds. All values in μm.

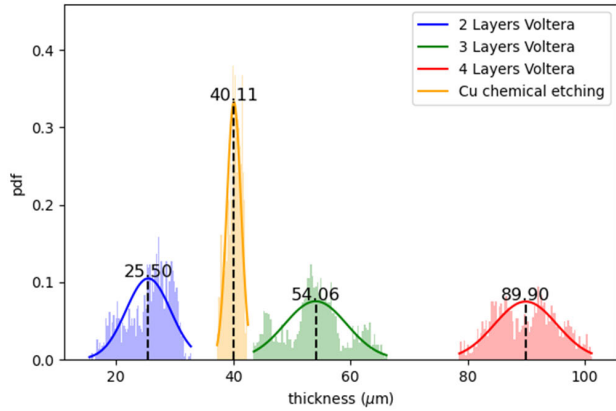| Batch	MEAN	STANDARD DEVIATION
2-layer SC-ink	25.49	3.80
3-layer SC-ink	54.06	5.29
4-layer SC-ink	89.90	5.32
Copper	40.10	1.19

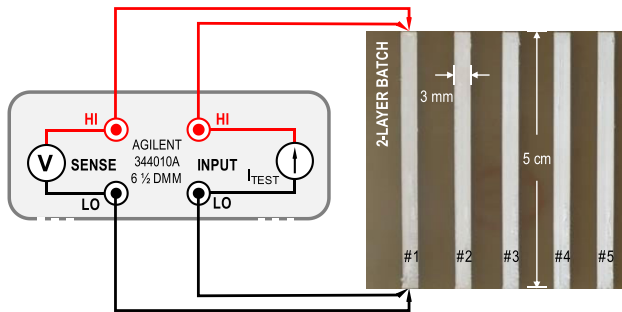**FIGURE 4.** Thickness probability density function (pdf).

FIGURE 5. 4-wire resistance measurement setup.

results in the most homogeneous or reliable on terms of thickness dispersion. Regarding the circuits made with 2, 3 and 4 layers of SC ink, the pattern of the distributions depends on the number of layers and the bending of the circuit, but the difference in thickness (between 30 and 35 μm) is similar to the nominal thickness programmed in the printing device. Actually, the tolerance in thickness achieved by the printer is similar to that of the cooper layers provided by commercial manufacturers.

B. DC ELECTRICAL CHARACTERIZATION

Electrical resistance was measured to an accuracy of ± 3 mΩ with a 6 1/2 digit multimeter (Agilent, model 34401A) using the four-wire technique. Fig. 5 shows the experimental setup for the resistance measurements and an image of the 2-layer SC-ink batch. The test current flows from the input HI terminal and then through the trace being measured (#1 in Fig. 5). The voltage drop across the trace is detected through

TABLE 2. Measured trace resistance. All values in mΩ.

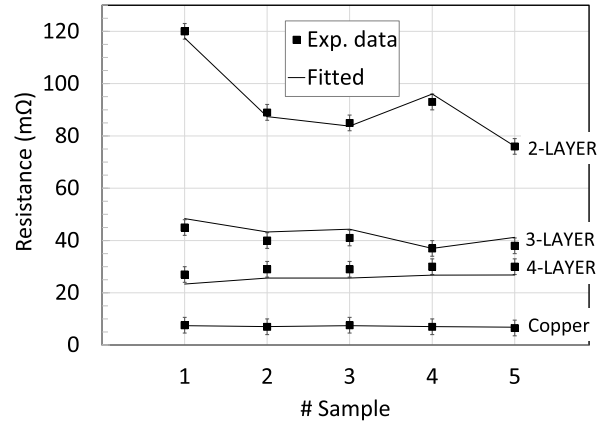| Batch	#1	#2	#3	#4	#5
2-layer SC-ink	120	89	85	93	76
3-layer SC-ink	45	40	41	37	38
4-layer SC-ink	27	29	29	30	30
Copper	7.6	7.0	7.6	7.0	6.5

FIGURE 6. DC resistance measured and fitted values for different silver-conductive ink print passes.

separate "sense" connections. Since no current flows in the sense leads, the resistance in these leads does not give a measurement error.

The results for the three batches of SC-ink traces and the one of copper traces are summarized in Table 2. At first glance, the results seem consistent: on the one hand, the thicker SC-ink traces show a lower resistance and, on the other hand, the copper traces show a much lower resistance, in agreement with the higher conductivity of copper.

From structural analysis of traces (Table 1) the mean thickness and standard deviation of each batch are taken and used in a fitting procedure to estimate the SC ink conductivity, σ_{DC}, assuming that the electrical resistance of a printed trace is given by:

$$R = \frac{l}{\sigma_{DC} \cdot w \cdot t} \tag{1}$$

where R is the trace electrical resistance, l, w, and t are trace length, width and thickness, respectively.

The fitting procedure uses all individual trace thicknesses and a single σ_{DC} as fitting parameters under the constraints imposed by the mean thickness and standard deviation for each batch and the uncertainty of the digital multimeter. The result of the fitting procedure is shown in Fig. 6 along with the experimental results for comparison.

The fit of the experimental data yields a conductivity value of $\sigma_{DC} = 7.25 \times 10^6$ S/m and trace thickness values given in Table 3. This value is only 8% lower than specified by the ink manufacturer (7.91×10^6 S/m $= 1/1.265 \times 10^{-7}$ Ωm). This small difference may be due to solvent loss in the time

TABLE 3. Individual fitted trace thickness from resistance measurements. All values in μm.

| Batch	#1	#2	#3	#4	#5	Mean	Std Dev
2-layer SC-ink	20	26	27	24	30	25.49	3.80
3-layer SC-ink	47	53	52	62	56	54.06	5.29
4-layer SC-ink	99	90	90	86	86	89.90	5.32
Copper	39	41	39	41	42	40.10	1.19

between dispensing and curing or while ink storage in the container after first opening.

The same fitting procedure was followed for the copper traces, yielding a conductivity value of 5.82×10^7 S/m, which perfectly matches its standard value. This is an indication that the method followed to obtain the SC ink conductivity is adequate.

C. ELECTRICAL CHARACTERIZATION AT MICROWAVE FREQUENCIES

Since a low-cost substrate is used in this work, before proceeding to analyze the suitability of SC ink at microwave frequencies, a substrate characterization has been performed. It is well known that FR4 type substrates exhibit a dielectric constant, ε_r, and a loss tangent, $\tan\delta$, which are around 4.4 and 0.02, respectively, at 1 GHz [44]. However, accurate values of these characteristics are required when designing circuits at microwave frequencies. We designed two basic types of circuits widely used for this purpose: a long microstrip line, commonly used to determine substrate losses, and a T-resonator, which is used to accurately determine the substrate dielectric constant [45]. On the other hand, SC-ink conductivity at microwave frequencies, σ_{RF}, is an unknown and is expected to be lower than its DC value, σ_{DC}, due to, among other reasons, surface roughness and width irregularities [38]. To estimate $\tan\delta$ and σ_{RF}, two 50-Ω microstrip lines of 10 cm length (2.90 mm nominal width) were fabricated: one copper-based by standard etching technique and the other by direct SC-ink writing. As mentioned, to estimate ε_r, a 50-Ω open ended quarter-wavelength microstrip resonator (50-mm port-to-port length and 30-mm stub length) was fabricated by direct SC-ink writing. Both the resonator and the 50-Ω line manufactured by direct-writing were fabricated by depositing two print passes of SC ink on the top of the board while the copper cladding on the bottom was left as a ground plane. The microstrip lines and resonator were connectorized with panel-edge SMA connectors.

Scattering parameters were measured from 500 kHz to 6 GHz using a Vector Network Analyzer (VNA) (Keysight model P9371A). SOLT calibration was performed on the input/output PCB edge-mount SMA connectors, as shown in Fig. 7. Therefore, connector and coaxial-to-microstrip transition effects are not removed from measured response and have some influence on the measurement results, as will be discussed later. These results were compared with simulations of the same circuits. These simulations were
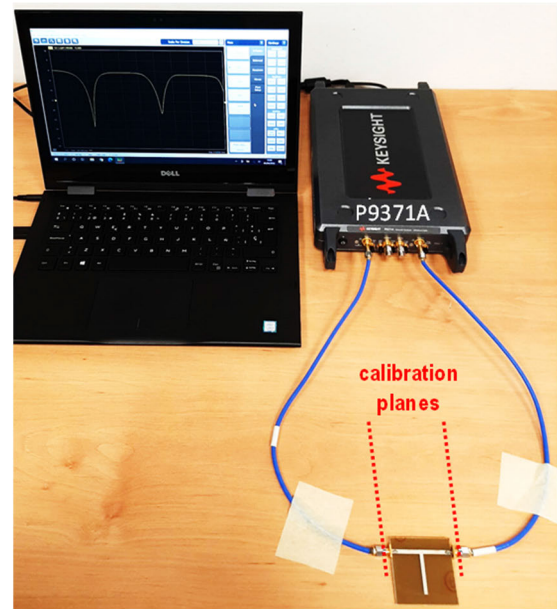
FIGURE 7. Experimental setup for RF characterization.

performed using ADS Momentum (Keysight Technologies) which is a 3D-planar electromagnetic solver based on the method of moments and is widely used for the analysis of passive microwave circuits.

For SC ink, the previously estimated conductivity value $\sigma_{DC} = 7.3 \times 10^6$ S/m was initially used, while the standard value of 5.8×10^7 S/m was used for copper. Microstrip line thickness was taken as 25 and 40 μm for SC ink and copper, respectively, according to the previously estimated values.

Fig. 8(a) shows measured transmission parameter, S_{21}, along with the simulated values for the SC ink T-resonator. A value of $\varepsilon_r = 4.35$ was used in order to obtain good agreement between the experimental and simulated resonance frequencies. Fig. 8(b) shows the comparison between measured and simulated reflection parameters, S_{11}, which shows some discrepancy in the response between resonance frequencies if SMA-to-microstrip transition is not corrected.

Fig. 9 shows the measured S_{21} and S_{11} parameters along with the simulated values for the copper microstrip line. A value of $\tan\delta = 0.019$ for the substrate loss tangent was adequate to get best agreement between experimental and simulated S_{21} parameter slopes in the low frequency range (below 3 GHz). The comparison between experimental and simulated behaviors above 3 GHz shows the effect of uncorrected SMA-to-microstrip transitions. Majewski et al. [46] proposed a well-established model for coax-to-microstrip transitions consisting of a reactive π-network (see inset in Fig. 9). In this case, a 0.55 nH series inductor and a 30 fF parallel capacitor on the coaxial line side proved to be the best choice to fit the data. The parallel capacitor on the microstrip side proved to be negligible. By introducing these parasitics in the simulations, excellent agreement is achieved in the S_{11} and S_{21} parameters over the whole frequency range, as it
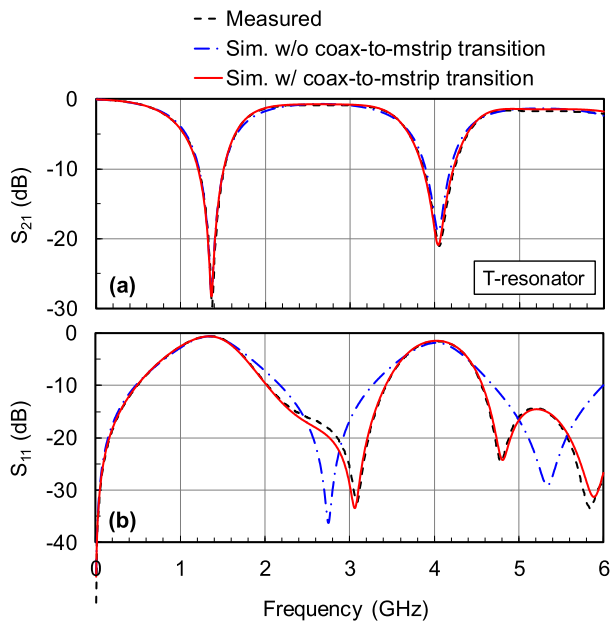
FIGURE 8. SC-ink resonator (a) transmission and (b) reflection S parameters. Comparison between measured data (dashed lines) and simulations is done both without (dot-dashed lines) and with coax-to-microstrip transition correction (solid lines).
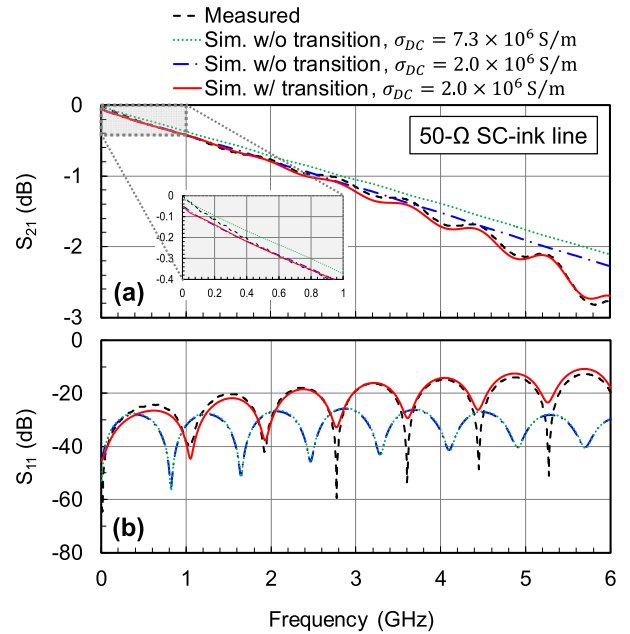

FIGURE 10. 50-Ohm SC-ink line (a) transmission and (b) reflection S parameters. Comparison between measured data (dashed lines) and simulations is done both without (dot-dashed lines) and with coax-to-microstrip transition correction (solid lines).
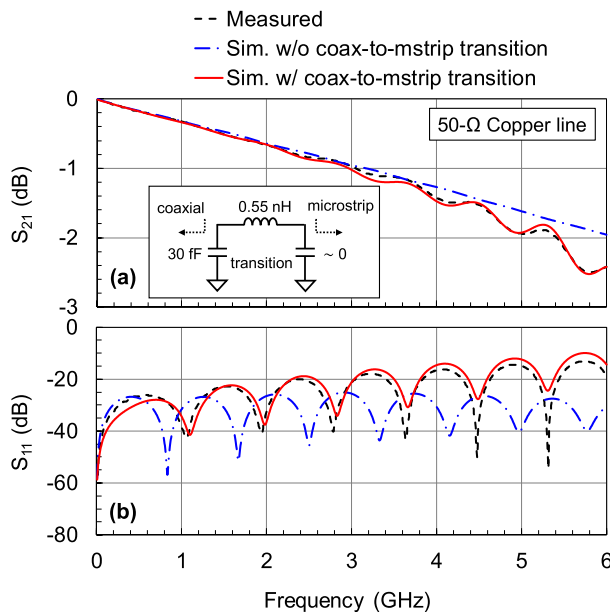

FIGURE 9. 50-Ohm copper line (a) transmission and (b) reflection S parameters. Comparison between measured data (dashed lines) and simulations is done both without (dot-dashed lines) and with coax-to-microstrip transition correction (solid lines).

same $\tan \delta$ value of 0.019 was used to maintain consistency with the copper line results. When comparing both lines, as expected for this type of substrate, both responses exhibit high losses due primarily to dielectric losses. The contribution of the conductor losses is evidenced by the small difference between the two responses and comes from the lower conductivity of the SC ink. The results indicate that a conductivity value of 7.3×10^6 S/m (dotted line) is consistent at the lowest frequency (see inset of Fig. 10(a)). However, at higher frequencies the results suggest that the conductivity of the SC ink is lower than its DC value σ_{DC}. This can be explained if the surface roughness of the conductor surface is taken into account. Effective conductivity, σ_{RF}, is a concept which is defined as the conductivity of a conductor with ideally smooth surface that would result in the same loss as the rough surface [47]. Although effective conductivity decreases with increasing frequency, using an average value of 2×10^6 S/m yields consistent results with RF simulations above 500 MHz. A similar decrease in RF effective conductivity has been reported in the literature for this type of ink [37], [38]. Fig. 10 also highlights the effect of properly including transition parasitics.

IV. DIRECT-WRITE MICROWAVE CIRCUITS PROOF OF CONCEPT
As a continuation of the process of validating the use of the low cost DIW system for microwave circuit fabrication, three circuits have been designed, simulated and fabricated. Based on the previous RF characterization, the circuits in this
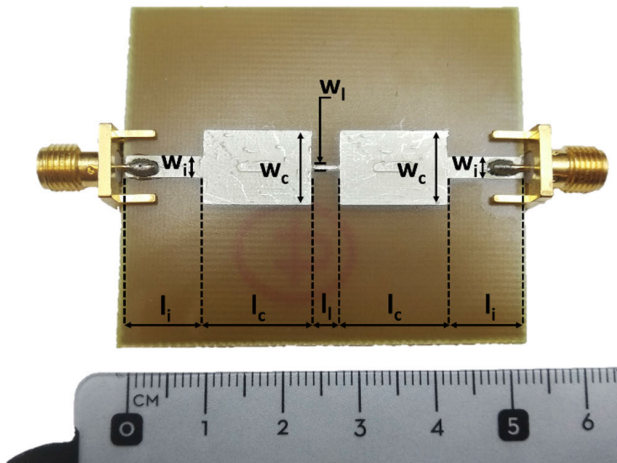
can be seen in Fig. 9. The same parasitics were considered in the resonator simulations achieving this time an excellent agreement on both, S$_{21}$ and S$_{11}$ parameters, as shown in Fig. 8 (solid line).

Fig. 10 shows the measured S$_{21}$ and S$_{11}$ parameters along with the simulated values for SC ink microstrip line. The

FIGURE 11. Fabricated stepped-impedance low-pass filter.

TABLE 4. Stepped-impedance low-pass filter dimensions.

Parameter	Value (mm)	Parameter	Value (mm)
w_i	2.90	l_i	10.00
w_l	0.50	l_l	3.68
w_c	10.00	l_c	13.84

section have been simulated using the values $\varepsilon_r = 4.35$, $\tan \delta = 0.019$ and $\sigma_{RF} = 2.0 \times 10^6$ S/m and including the same coaxial-to-microstrip transition parasitics as before.

A. MICROSTRIP STEPPED IMPEDANCE LOW PASS FILTER

The first of the circuits evaluated is a stepped-impedance (SI) low pass (LP) filter consisting of alternating sections of very high and very low characteristic impedance lines. It is a 3rd order Chebyshev LP filter with 3-dB ripple and a cutoff frequency of 2.5 GHz, and was designed by the insertion loss method using simple well-known expressions [48], without any further refinement, since the objective was to demonstrate to what extent the fabricated filter behaved like the simulated nominal one. The widths of the high and low impedance lines (w_l and w_c) were chosen to be 0.5 mm and 10 mm, respectively. Fig. 11 shows the fabricated SI-LP filter along with the definition of the dimension parameters, the values of which are given in Table 4.

As can be clearly seen in Fig. 12, the resulting cutoff frequency is well below the design frequency, due to the approximations underlying this method for this type of filter (wide lines should behave like ideal capacitors, but they have a length such that their inductive components are not negligible). In fact, the EM simulation of this filter makes this clear. The measured and simulated results are very similar over the entire frequency range evaluated, demonstrating that the DIW system is reliable in this frequency range for designs that present features within manufacturing tolerances, as is the case
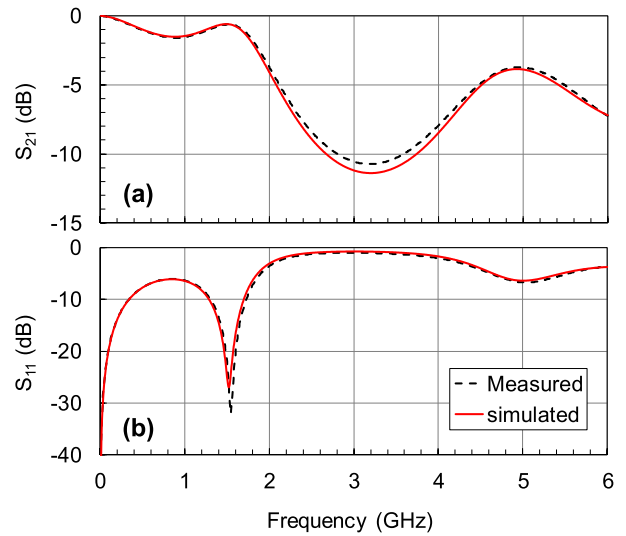

FIGURE 12. Comparison between experimental data (dashed lines) and simulations (solid lines) of (a) S_{21} and (b) S_{11} parameters for the stepped-index low-pass filter.
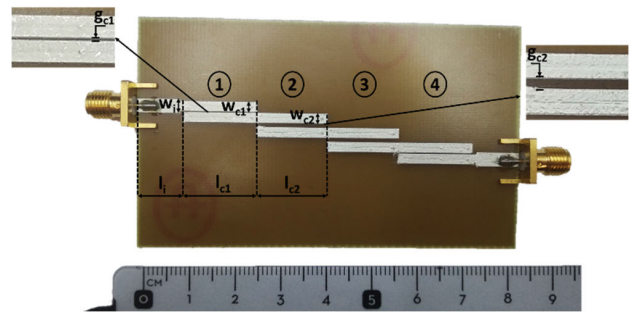

FIGURE 13. Fabricated coupled-line band-pass filter.

B. MICROSTRIP COUPLED LINE BANDPASS FILTER

The second of the circuits evaluated is a 3rd order coupled-line band-pass (BP) filter. It has been designed following a classical Chebyshev approximation with 3-dB ripple, a center frequency of 2.7 GHz and a fractional bandwidth of 10% [48]. Fig. 13 shows the fabricated BP filter based on four quarter-wavelength coupled line sections along with the definition of dimension parameters, whose values are listed in Table 5. The coupled line sections 1 and 2 are equal to sections 4 and 3, respectively. It is evident that the value of the gap parameter g_{c1} (0.32 mm) is well below the Voltera's specification for clearance (0.65 mm). Therefore, this design is worthwhile to explore the limit of this printing system's capability for track clearance.

Fig. 14 shows the comparison between measured and simulated S_{21} and S_{11} parameters of this filter, showing a reasonably good agreement. However, it is clear that the measured response (dashed line) has wider bandwidth. This is possibly due to SC-ink spreading which, in turn, causes the spacing between the coupled lines to be reduced. Further simulations confirm that an increase in line width of only 50 μm (and

TABLE 5. Coupled-line band-pass filter dimensions.

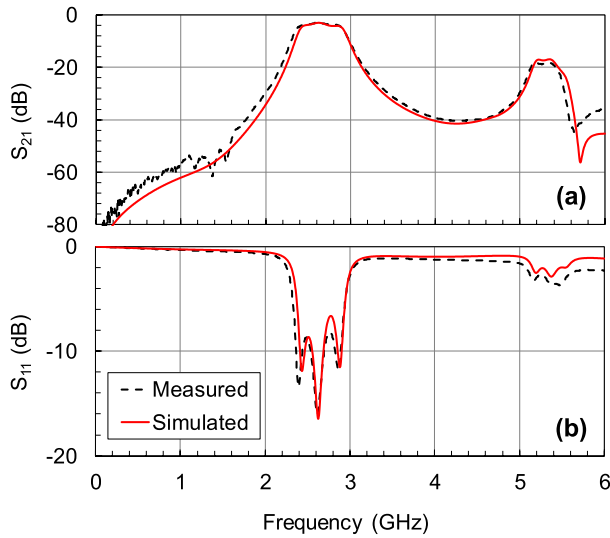| Parameter	Value (mm)	Parameter	Value (mm)
w_i	2.90	l_i	10.00
w_{c1}	2.07	l_{c1}	15.78
g_{c1}	0.32	l_{c1}	15.41
w_{c2}	2.18	g_{c2}	1.07

FIGURE 14. Comparison between experimental data (dashed lines) and simulations (solid lines) of (a) S_{21} and (b) S_{11} parameters for the coupled-line band-pass filter.
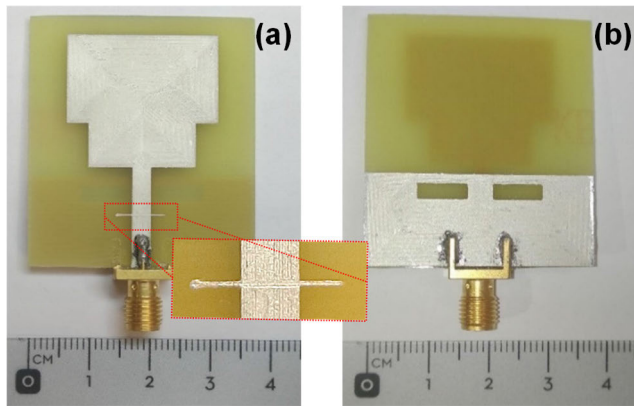

FIGURE 15. (a) Top, and (b) bottom views of the UWB antenna.

a consequent reduction in spacing of 100 μm) will result in an increase in bandwidth similar to that measured. Line widening of this magnitude has been reported in [49] for the Voltera V-One system.

C. BROADBAND MONOPOLE PRINTED ANTENNA

Finally, in order to demonstrate the feasibility of this low-cost manufacturing system for RF applications beyond 6 GHz, we have fabricated a SC ink patch monopole antenna for UWB applications that was already designed, fabricated and reported by authors for copper standard etching procedure
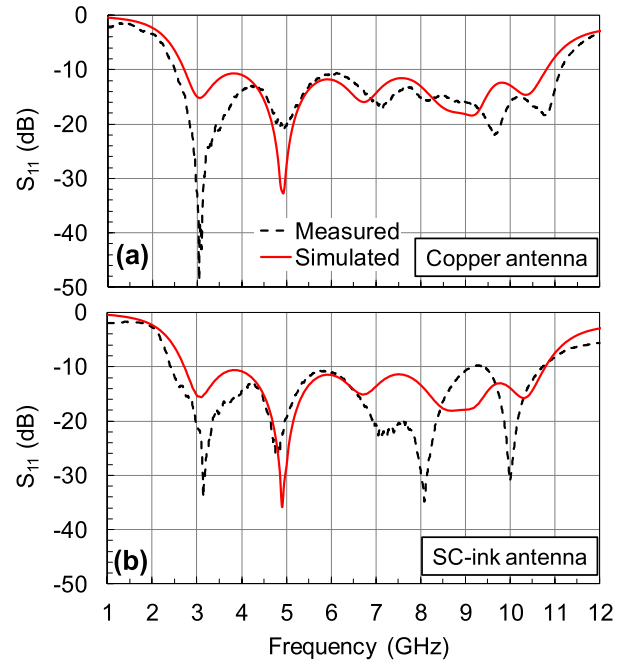

FIGURE 16. Measured (dashed lines) and simulated (solid lines) S_{11} parameters for (a) copper and (b) SC ink antennas.

TABLE 6. Simulated and measured antenna gain.

Frequency (GHz)	Copper antenna Gain (dBi)		SC-ink antenna Gain (dBi)	
	Simulated	Measured	Simulated	Measured
3.0	2.1	1.3	2.1	1.2
4.5	2.7	2.8	2.6	2.7
6.0	4.4	4.2	4.3	4.1
7.5	5.7	5.3	5.6	5.2
9.0	5.4	4.6	5.4	4.3
10.5	7.3	6.6	7.1	6.3

[39]. Both sides of the design are presented in Fig. 15 and detailed dimensions can be found in [39]. It is a printed stepped-type monopole antenna with two rectangular slots added on the ground plane and two strips added to the top layer feeding line resulting in bandwidth enhancement. The antenna has a total size of 40 mm × 36 mm and features omnidirectional radiation and a maximum gain of 6.6 dBi. The choice of this antenna as a test circuit for the use of the DIW system is motivated to its already proven wide bandwidth ($S_{11} < -10$ dB), between 2.7 and 11.4 GHz, i.e., 8.7 GHz bandwidth.

The antenna was manufactured entirely by SC-ink DIW, i.e., SC ink was deposited on both sides of the board: first the top side of the antenna was deposited and cured, and then the bottom side (or ground layer) was deposited and cured. As mentioned above, to ensure the alignment of the circuit on both sides, some control points were added to the design to allow the correct positioning of the printer head, which were subsequently removed.

TABLE 7. Comparison with previous works on DIW of silver conductive ink.

Work Ref	Conductor	Substrate	Ink/substrate electrical characterization	Conductivity value used in simulations	Devices/frequency	Applications
[8]	SC-ink	Kapton FR4	No	Not explicitly mentioned	Dual band antennas 2.5 – 4.5 GHz	Wireless power transfer
[24]	SC-ink	Kapton	No	σ_{DC}: 1.05×10^6 S/m	CPW Antenna 2.4 GHz	Wearable electronics
[25]	SC-ink	Kapton	No	σ_{RF}: 2×10^5 S/m	Rectenna 0.9 – 0.94 GHz	RF Energy harvesting
[26]	SC-ink	Glass	No	σ_{DC}: 1.05×10^6 S/m	Slot antenna 2.4 GHz	Wearable electronics
[38]	CNC veil [a] SC-ink	Structural glass	σ_{RF} on Rogers 5880 Up to 6.5 GHz	σ_{RF}: 2×10^6 S/m (CNC veil) 1.05×10^6 S/m (SC-ink)	RF-switch IL: 3dB @ ~5.5 GHz, > 4dB @ 8.5 GHz	Active RF switches
[50], [51]	Silver epoxy-based ink	Polyester fabric	σ_{DC}	σ_{DC}: 9.97×10^4 – 2.0032×10^5 S/m	Patch antenna 1.575 GHz	Wearable electronics
This Work	SC-ink	FR4	σ_{DC} ε_r, $\tan\delta$, σ_{RF} Up tp 6 GHz	σ_{DC}: 7.25×10^6 S/m σ_{RF}: 2×10^6 S/m	UWB antenna 2.4 – 10.6 GHz	Medical imaging

[a] CNC: carbon–nickel–copper

The antenna was simulated using 3D electromagnetic simulation software EMPro (Keysight Technologies), which is widely used in the design of antennas of this type. The simulation considered the same property values used previously for both the substrate and the SC ink.

In this case, S_{11} parameters were measured using a 40-GHz VNA (Agilent model E8363B). Fig. 16 shows the comparison between measured (dashed lines) and simulated (solid lines) results for the printed antenna from 1 to 12 GHz. Fig. 16(a) and (b) displays copper antenna and SC ink antenna results, respectively. The simulated S_{11} parameters of the two antennas show very small differences, demonstrating that the lower conductivity of the SC ink is not a problem. With regard to the measured behavior, comparing the measurements obtained with both manufacturing methods, it is observed that at low and medium frequencies, both antennas show very similar responses. Also, a somewhat different behavior is observed at higher frequencies: around 8 and 10 GHz there are minima in the SC-ink printed antenna that are not observed in the copper antenna. This could be due to a faulty ink deposition when forming the critical cross-line strips as these two elements are only 0.3 mm wide with 45° beveled ends [49], outside the scope of Voltera's manufacturing capability. A zoomed view of these two elements in Fig. 15 shows that there is no trace of the beveled ends. In fact, the end of one of the strips is rounded with an SC ink bulge. According to [39], these two strips originate a resonance around 9 GHz and this reinforces the idea that the imperfection of the deposition justifies the experimental minima appearing around 8 and 10 GHz.

As for de gain, the radiation patterns of the SC ink antenna were simulated and measured. Table 6 presents the gain values for frequencies within the antenna bandwidth. There is a great similarity between the results for the copper antenna and for the SC-ink antenna, mainly due to the fact that the radiation patterns depend primarily on the geometry of the

antenna. A maximum reduction of only 0.3 dB has been obtained at the highest frequency, due to the ohmic losses of the SC ink. This is explained by the higher ohmic losses of SC ink compared to copper, which in turn reduces the efficiency of the antenna and thus the gain.

From the above, it is concluded that the performance of the SC-ink fabricated antenna corresponds quite well with that of the simulations, demonstrating the validation of this low-cost SC-ink direct writing system for microwave designs up to 10.6 GHz, which was the main objective of this work.

In order to highlight the advantages of our work, we have made a comparison with similar previously published research papers. Table 7 lists some representative ones reporting on both measurements and simulations of RF circuits. We found that most of the previous works using DIW of SC-ink in RF applications focus on the realization of antennas of some kind for wireless power transfer and wearable electronics applications up to 4.5 GHz, such as [8], [24], [25], and [26]. All of them use in their simulations the bulk conductivity value given by the ink vendor. On the other hand, there are other studies that provide a prior characterization of SC-ink conductivity. This is the case of refs. [50] and [51] which report on a 1.575 GHz antenna whose performance strongly depends on the SC-ink losses, and a characterization of the bulk conductivity of the SC-ink as a function of the deposition conditions is performed with the objective of minimizing the track resistance. Finally, it is also included a work on an RF switch [38] in which an SC-ink characterization up to 6.5 GHz is performed. In [38] a comparison is made between the behavior of a CNC veil material and that of SC-ink. However, such characterization is carried out on a high frequency laminate (Rogers 5880), which is different from the one that is to be used in the final device (based on pre-peg material similar to FR4 in terms of dielectric constant and loss tangent). In the end, the RF part of the switching

circuit is made using the CNC veil because of its higher RF conductivity compared to SC-ink. In contrast to these previous studies, in this work we provide a comprehensive analysis of all circuit fabrication parameters using an SC-ink DIW system, accurately obtaining both the bulk conductivity and the RF effective conductivity of the SC-ink. Such detailed knowledge of material properties and fabrication constraints allows us to accurately design and simulate RF circuits and increase the frequency band of use of low-cost DIW circuits up to 10 GHz.

V. CONCLUSION

A low-cost prototyping system has been presented based on SC-ink DIW and standard FR4 substrates for RF applications.

Different test circuits were chosen and fabricated to, first, properly characterize the SC ink and substrate and, second, explore the limits of reliable fabrication for track clearance, line width and challenging geometries. It has been demonstrated that the use of a simple DIW system together with suitable SC-ink and substrate characterization methods can be applied to the reliable fabrication of circuits operating up to 10.6 GHz, such as the reported SC ink DIW UWB antenna, having a bandwidth between 2.4 and 10.6 GHz. Surface roughness and irregularities in the width of the conductive ink lines lead to an effective decrease in ink conductivity with a consequent increase in conductor losses, and should be addressed for the proper circuit design at microwave frequencies. It was also pointed that the employed DIW system had some drawbacks, such as ink spreading and thickening at the end of the lines, which could potentially jeopardize the reliable manufacturability of both line clearance and width below 0.3 mm, and this should be taken into account for any future designs.

It should be noted that SC ink could be deposited by DIW on specific high frequency substrates. In this sense, the frequency range could be further extended by characterizing the conductivity of SC ink at higher frequencies. However, it should be emphasized that the great utility of these DIW systems lies in the use of low-cost materials.

REFERENCES

[1] T. Srivatsan and T. Sudarshan, *Additive Manufacturing: Innovations, Advances, and Applications*. Boca Raton, FL, USA: CRC Press, 2015, doi: 10.1201/b19360.

[2] J. Persad and S. Rocke, "A survey of 3D printing technologies as applied to printed electronics," *IEEE Access*, vol. 10, pp. 27289–27319, 2022, doi: 10.1109/ACCESS.2022.3157833.

[3] J. Wiklund, A. Karakoç, T. Palko, H. Yiğitler, K. Ruttik, R. Jäntti, and J. Paltakari, "A review on printed electronics: Fabrication methods, inks, substrates, applications and environmental impacts," *J. Manuf. Mater. Process.*, vol. 5, no. 3, p. 89, Aug. 2021, doi: 10.3390/jmmp5030089.

[4] E. Macdonald, R. Salas, D. Espalin, M. Perez, E. Aguilera, D. Muse, and R. B. Wicker, "3D printing for the rapid prototyping of structural electronics," *IEEE Access*, vol. 2, pp. 234–242, 2014, doi: 10.1109/ACCESS.2014.2311810.

[5] H. García-Martínez, E. Ávila-Navarro, G. Torregrosa-Penalva, A. Rodríguez-Martínez, C. Blanco-Angulo, and M. A. D. L. De La Casa-Lillo, "Low-cost additive manufacturing techniques applied to the design of planar microwave circuits by fused deposition modeling," *Polymers*, vol. 12, no. 9, p. 1946, Aug. 2020, doi: 10.3390/polym12091946.

[6] M. Schouten, G. Wolterink, A. Dijkshoorn, D. Kosmas, S. Stramigioli, and G. Krijnen, "A review of extrusion-based 3D printing for the fabrication of electro- and biomechanical sensors," *IEEE Sensors J.*, vol. 21, no. 11, pp. 12900–12912, Jun. 2021, doi: 10.1109/JSEN.2020.3042436.

[7] J. S. Chang, A. F. Facchetti, and R. Reuss, "A circuits and systems perspective of organic/printed electronics: Review, challenges, and contemporary and emerging design approaches," *IEEE J. Emerg. Sel. Topics Circuits Syst.*, vol. 7, no. 1, pp. 7–26, Mar. 2017, doi: 10.1109/JETCAS.2017.2673863.

[8] M. Haerinia and S. Noghanian, "A printed wearable dual-band antenna for wireless power transfer," *Sensors*, vol. 19, no. 7, p. 1732, Apr. 2019, doi: 10.3390/s19071732.

[9] S. Khan, L. Lorenzelli, and R. S. Dahiya, "Technologies for printing sensors and electronics over large flexible substrates: A review," *IEEE Sensors J.*, vol. 15, no. 6, pp. 3164–3185, Jun. 2015, doi: 10.1109/JSEN.2014.2375203.

[10] M. E. Morales-Rodriguez, P. C. Joshi, J. R. Humphries, P. L. Fuhr, and T. J. Mcintyre, "Fabrication of low cost surface acoustic wave sensors using direct printing by aerosol inkjet," *IEEE Access*, vol. 6, pp. 20907–20915, 2018, doi: 10.1109/ACCESS.2018.2824118.

[11] M. Baghelani, Z. Abbasi, M. Daneshmand, and P. E. Light, "Non-invasive continuous-time glucose monitoring system using a chipless printable sensor based on split ring microwave resonators," *Sci. Rep.*, vol. 10, no. 1, p. 12980, Jul. 2020, doi: 10.1038/s41598-020-69547-1.

[12] M. El Gharbi, R. Fernández-García, S. Ahyoud, and I. Gil, "A review of flexible wearable antenna sensors: Design, fabrication methods, and applications," *Materials*, vol. 13, no. 17, p. 3781, Aug. 2020, doi: 10.3390/ma13173781.

[13] M. Shakeel, K. Rehman, S. Ahmad, K.-H. Choi, and A. Khan, "A weldless approach for thermocouple fabrication through direct ink writing technique," *IEEE Sensors J.*, vol. 21, no. 2, pp. 1279–1286, Jan. 2021, doi: 10.1109/JSEN.2020.3018747.

[14] S. Singh, Y. Takeda, H. Matsui, and S. Tokito, "Flexible PMOS inverter and NOR gate using inkjet-printed dual-gate organic thin film transistors," *IEEE Electron Device Lett.*, vol. 41, no. 3, pp. 409–412, Mar. 2020, doi: 10.1109/LED.2020.2969275.

[15] V. Subramanian, J. M. J. Frechet, P. C. Chang, D. C. Huang, J. B. Lee, S. E. Molesa, A. R. Murphy, D. R. Redinger, and S. K. Volkman, "Progress toward development of all-printed RFID tags: Materials, processes, and devices," *Proc. IEEE*, vol. 93, no. 7, pp. 1330–1338, Jul. 2005, doi: 10.1109/JPROC.2005.850305.

[16] J. Fernández-Salmerón, A. Rivadeneyra, F. Martínez-Martí, L. Capitán-Vallvey, A. Palma, and M. Carvajal, "Passive UHF RFID tag with multiple sensing capabilities," *Sensors*, vol. 15, no. 10, pp. 26769–26782, Oct. 2015, doi: 10.3390/s151026769.

[17] N. A. Shepelin, P. C. Sherrell, E. Goudeli, E. N. Skountzos, V. C. Lussini, G. W. Dicinoski, J. G. Shapter, and A. V. Ellis, "Printed recyclable and self-poled polymer piezoelectric generators through single-walled carbon nanotube templating," *Energy Environ. Sci.*, vol. 13, no. 3, pp. 868–883, Mar. 2020, doi: 10.1039/C9EE03059J.

[18] Y. Yan, C. Ding, K. D. T. Ngo, Y. Mei, and G.-Q. Lu, "Additive manufacturing of planar inductor for power electronics applications," in *Proc. Int. Symp. 3D Power Electron. Integr. Manuf. (3D-PEIM)*, Jun. 2016, pp. 1–16, doi: 10.1109/3DPEIM.2016.7570536.

[19] G. Beziuk, T. C. Baum, K. Ghorbani, and K. J. Nicholson, "Multi-functional composite RF four-way switch," in *IEEE MTT-S Int. Microw. Symp. Dig.*, Jun. 2019, pp. 1088–1091, doi: 10.1109/MWSYM.2019.8700866.

[20] C. Reig and E. Ávila-Navarro, "Printed antennas for sensor applications: A review," *IEEE Sensors J.*, vol. 14, no. 8, pp. 2406–2418, Aug. 2014, doi: 10.1109/JSEN.2013.2293516.

[21] J. M. Hoey, M. T. Reich, A. Halvorsen, D. Vaselaar, K. Braaten, M. Maassel, I. S. Akhatov, O. Ghandour, P. Drzaic, and D. L. Schulz, "Rapid prototyping RFID antennas using direct-write," *IEEE Trans. Adv. Packag.*, vol. 32, no. 4, pp. 809–815, Nov. 2009, doi: 10.1109/TADVP.2009.2021768.

[22] P. Njogu, B. Sanz-Izquierdo, A. Elibiary, S. Y. Jun, Z. Chen, and D. Bird, "3D printed fingernail antennas for 5G applications," *IEEE Access*, vol. 8, pp. 228711–228719, 2020, doi: 10.1109/ACCESS.2020.3043045.

[23] W. G. Whittow, A. Chauraya, J. C. Vardaxoglou, Y. Li, R. Torah, K. Yang, S. Beeby, and J. Tudor, "Inkjet-printed microstrip patch antennas realized on textile for wearable applications," *IEEE Antennas Wireless Propag. Lett.*, vol. 13, pp. 71–74, Jan. 2014, doi: 10.1109/LAWP.2013.2295942.

[24] M. Wagih, "Direct-write dispenser printing for rapid antenna prototyping on thin flexible substrates," in *Proc. 14th Eur. Conf. Antennas Propag. (EuCAP)*, Mar. 2020, pp. 1–4, doi: 10.23919/EuCAP48036.2020.9135625.

[25] M. Wagih, A. S. Weddell, and S. Beeby, "Meshed high-impedance matching network-free rectenna optimized for additive manufacturing," *IEEE Open J. Antennas Propag.*, vol. 1, pp. 615–626, 2020, doi: 10.1109/OJAP.2020.3038001.

[26] E. Cil and S. Dumanli, "The design of a reconfigurable slot antenna printed on glass for wearable applications," *IEEE Access*, vol. 8, pp. 95417–95423, 2020, doi: 10.1109/ACCESS.2020.2996020.

[27] C. Blanco-Angulo, A. Martínez-Lozano, R. Gutiérrez-Mazón, C. G. Juan, H. García-Martínez, J. Arias-Rodríguez, J. M. Sabater-Navarro, and E. Ávila-Navarro, "Non-invasive microwave-based imaging system for early detection of breast tumours," *Biosensors*, vol. 12, no. 9, p. 752, Sep. 2022, doi: 10.3390/bios12090752.

[28] H. Li, H. Zhang, Y. Kong, and C. Zhou, "Flexible dual-polarized UWB antenna sensors for breast tumor detection," *IEEE Sensors J.*, vol. 22, no. 13, pp. 13648–13658, Jul. 2022, doi: 10.1109/JSEN.2022.3180356.

[29] N. AlSawaftah, S. El-Abed, S. Dhou, and A. Zakaria, "Microwave imaging for early breast cancer detection: Current state, challenges, and future directions," *J. Imag.*, vol. 8, no. 5, p. 123, Apr. 2022, doi: 10.3390/jimaging8050123.

[30] R. V. K. Rao, K. V. Abhinav, P. S. Karthik, and S. P. Singh, "Conductive silver inks and their applications in printed and flexible electronics," *RSC Adv.*, vol. 5, no. 95, pp. 77760–77790, 2015, doi: 10.1039/C5RA12013F.

[31] P. Escobedo, M. A. Carvajal, J. Banqueri, A. Martínez-Olmos, L. F. Capitán-Vallvey, and A. J. Palma, "Comparative study of inkjet-printed silver conductive traces with thermal and electrical sintering," *IEEE Access*, vol. 7, pp. 1909–1919, 2019, doi: 10.1109/ACCESS.2018.2887113.

[32] B. M. Nikolova, E. E. Gieva, G. T. Nikolov, I. N. Ruskova, and M. G. Mladenov, "Sintering temperature impact on sheet resistance of inkjet printed layers," in *Proc. X Nat. Conf. Int. Participation (ELECTRONICA)*, May 2019, pp. 1–4, doi: 10.1109/ELECTRONICA.2019.8825642.

[33] S. Wünscher, T. Rasp, M. Grouchko, A. Kamyshny, R. M. Paulus, J. Perelaer, T. Kraft, S. Magdassid, and U. S. Schubert, "Simulation and prediction of the thermal sintering behavior for a silver nanoparticle ink based on experimental input," *J. Mater. Chem. C*, vol. 2, no. 31, pp. 6342–6352, 2014, doi: 10.1039/C4TC00632A.

[34] P. Jiang, Z. Ji, X. Zhang, Z. Liu, and X. Wang, "Recent advances in direct ink writing of electronic components and functional devices," *Prog. Addit. Manuf.*, vol. 3, pp. 65–86, 2018, doi: 10.1007/s40964-017-0035-x.

[35] H. C. Rao, B. K. S. V. L. Varaprasad, and S. Goel, "Direct ink writing as an eco-friendly PCB manufacturing technique for rapid prototyping," in *Proc. 4th Int. Conf. Electr., Comput. Commun. Technol. (ICECCT)*, Sep. 2021, pp. 1–7, doi: 10.1109/ICECCT52121.2021.9616903.

[36] S. Vasquez, M. Petrelli, M. C. Angeli, J. Costa, E. Avancini, G. Cantarella, N. Munzenrieder, P. Lugli, and L. Petti, "Cost-effective, mask-less, and high-throughput prototyping of flexible hybrid electronic devices using dispense printing and conductive silver ink," in *Proc. 5th IEEE Electron Devices Technol. Manuf. Conf. (EDTM)*, Apr. 2021, pp. 1–3, doi: 10.1109/EDTM50988.2021.9420858.

[37] P. Pa, M. S. Mirotznik, and S. Yarlaggada, "High frequency characterization of conductive inks embedded within a structural composite," in *Proc. IEEE Int. Symp. Antennas Propag. USNC/URSI Nat. Radio Sci. Meeting*, Jul. 2015, pp. 1310–1311, doi: 10.1109/APS.2015.7305044.

[38] G. Beziuk, T. C. Baum, K. Ghorbani, and K. J. Nicholson, "RF signal multiplexer embedded into multifunctional composite structure," *IEEE Trans. Microw. Theory Techn.*, vol. 67, no. 12, pp. 4935–4943, Dec. 2019, doi: 10.1109/TMTT.2019.2944616.

[39] A. Martínez-Lozano, C. Blanco-Angulo, H. García-Martínez, R. Gutiérrez-Mazón, G. Torregrosa-Penalva, E. Ávila-Navarro, and J. M. Sabater-Navarro, "UWB-printed rectangular-based monopole antenna for biological tissue analysis," *Electronics*, vol. 10, no. 3, p. 304, Jan. 2021, doi: 10.3390/electronics10030304.

[40] A. Alemaryeen, "Compact wideband antenna for wireless capsule endoscopy system," *Appl. Phys. A, Solids Surf.*, vol. 127, no. 4, p. 271, Apr. 2021, doi: 10.1007/s00339-021-04420-0.

[41] S. Yan, P. J. Soh, and G. A. E. Vandenbosch, "Wearable ultrawideband technology—A review of ultrawideband antennas, propagation channels, and applications in wireless body area networks," *IEEE Access*, vol. 6, pp. 42177–42185, 2018, doi: 10.1109/ACCESS.2018.2861704.

[42] *The Voltera V-One Spec*. Voltera, ON, Canada. Accessed: Jun. 20, 2022. [Online]. Available: https://assets.ctfassets.net/e6vf9wdhbae5/2yjsp6sI8Zw7w2YN09oecH/892e3bb674cd4a38de84ba3bfe82951d/specs.pdf

[43] *Voltera Conductor 2 (1000388)*. Voltera, ON, Canada. Accessed: Jun. 20, 2022. [Online]. Available: https://assets.ctfassets.net/e6vf9wdhbae5/4kVMoPy3d4hmwGaCo17VU5/33130f6ffc1ab68abeae68721015b37a/Voltera_Standard_Conductor2_Ink__1000388_.pdf

[44] J. R. Aguilar, M. Beadle, P. T. Thompson, and M. W. Shelley, "The microwave and RF characteristics of FR4 substrates," in *Proc. IEE Colloq. Low Cost Antenna Technol. (Ref. no. 1998/206)*, Feb. 1998, p. 2, doi: 10.1049/ic:19980078.

[45] D. I. Amey and S. J. Horowitz, "Materials performance at frequencies up To 20 Ghz," in *Proc. IEMT/IMC Symp., 1st Joint Int. Electron. Manuf. Symp. Int. Microelectron. Conf.*, Apr. 1997, pp. 331–336.

[46] M. L. Majewski, R. W. Rose, and J. R. Scott, "Modeling and characterization of microstrip-to-coaxial transitions," *IEEE Trans. Microw. Theory Techn.*, vol. MTT-29, no. 8, pp. 799–805, Aug. 1981, doi: 10.1109/TMTT.1981.1130450.

[47] B. Huang and Q. Jia, "Accurate modeling of conductor rough surfaces in waveguide devices," *Electronics*, vol. 8, no. 3, p. 269, Mar. 2019, doi: 10.3390/electronics8030269.

[48] D. M. Pozar, "Microwave filters," in *Microwave Engineering*, 3rd ed. Hoboken, NJ, USA: Wiley, 2005, pp. 405–440.

[49] A. Zdrok, S. Artishchev, and A. Loschilov, "Experimental research of plotter printing of HIC thick-film conductors," in *Proc. ITM Web Conf.*, vol. 30, 2019, p. 07004, doi: 10.1051/itmconf/20193007004.

[50] R. K. Khirotdin, M. M. M. N. Nazli, M. A. Mahadzir, and N. Hassan, "Printing and curing of conductive inks on fabric using syringe-based deposition system and oven for wearable antenna application," *J. Phys., Conf.*, vol. 1150, Jan. 2019, Art. no. 012039, doi: 10.1088/1742-6596/1150/1/012039.

[51] R. K. Khirotdin, M. A. Mahadzir, F. C. Seman, S. H. Dahlan, and N. Hassan, "Performance evaluation of wearable antenna printed using syringe-based deposition system on fabric," *IOP Conf. Mater. Sci. Eng.*, vol. 607, no. 1, Aug. 2019, Art. no. 012010, doi: 10.1088/1757-899X/607/1/012010.

CAROLINA BLANCO-ANGULO was born in Alicante, Spain. She received the master's degree in telecommunication engineering from Miguel Hernández University of Elche, Spain, in 2020. She is currently pursuing the Ph.D. degree with the Department of Materials Science, Optics and Electronic Technology. Since 2018, she has been a Researcher at the Department of Materials Science, Optics and Electronic Technology. Her research interests include passive and active microwave devices and microwave imaging systems for tumor detection.

ANDREA MARTÍNEZ-LOZANO was born in Murcia, Spain. She received the bachelor's degree in telecommunication system engineering from the Catholic University San Antonio of Murcia (UCAM), Spain, in 2018, and the master's degree in telecommunication engineering from the Miguel Hernández University of Elche (UMH), Spain, in 2020. She is currently pursuing the Ph.D. degree with an ACIF research grant from the Valencian Regional Government. Since 2019, she has been a Researcher at the Department of Materials Science, Optics and Electronic Technology, UMH. Her current research interests include printed antennas, passive and active microwave devices, and microwave imaging systems for tumor detection.

JULIA ARIAS-RODRÍGUEZ received the M.Sc. degree in physics from the Universidad de Salamanca, in 1993, and the Ph.D. degree in science from the Universidad Politécnica de Madrid, in 1998. In 1999, she joined the Department of Materials, Optics and Electronic Technology, Universidad Miguel Hernández, Spain. Since 2001, she has been an Associate Professor of electronic technology. Her research covers a wide range of both experimental and theoretical activities in the fields of semiconductor lasers, in particular, high-power lasers and vertical-cavity surface-emitting lasers, multilayer dielectric optical filters, and wave propagation in anomalous dispersive media. Apart from the above, her current research interest includes theoretical and experimental printed microwave circuits for biomedical applications.

ALBERTO RODRÍGUEZ-MARTÍNEZ (Senior Member, IEEE) received the B.E. degree in telecommunications from the University of Vigo, Spain, in 1998, and the Ph.D. degree in telecommunications from the Polytechnic University of Valencia, Spain, in 2011. He is currently an Associate Professor with the Department of Communications Engineering, University Miguel Hernández of Elche, Elche, Spain. His research interests include time-to-frequency analysis, ultrasonic signals processing, for nondestructive materials characterization, and biomedical signal processing.
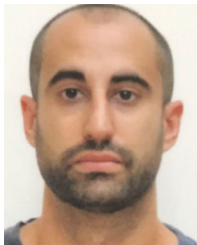
JOSÉ MARÍA VICENTE-SAMPER received the M.Sc. degree in industrial engineering and the Ph.D. degree in industrial and telecommunication technologies from Miguel Hernández University, Elche, Spain, in 2017 and 2021, respectively. Since 2015, he has been a Teaching Assistant and a Research Assistant with the Neuroengineering Biomedical Group, Bioengineering Institute, Miguel Hernández University.

JOSÉ MARÍA SABATER-NAVARRO (Senior Member, IEEE) received the M.Sc. degree in industrial engineering from the Polytechnic University of Valencia, Valencia, Spain, in 1998, and the Ph.D. degree from Miguel Hernández University, Elche, Spain, in 2003. He is currently a Full Professor with the Department of Systems Engineering and Automation and a Researcher of nBio Research Group. He received a Young Researchers Grant at the Chemical Institute (ITQ) CSIC-UPV, Polytechnic University of Valencia. His research is focused on the subjects of medical robotics and medical images. His main interests include surgical robotics, rehabilitation robotics, and medical computer applications for health.

ERNESTO ÁVILA-NAVARRO received the M.S. degree in telecommunication engineering from the Polytechnic University of Valencia, Valencia, Spain, in 1998, and the Ph.D. degree from Miguel Hernández University, Elche, Spain, in 2008. In 2000, he joined Miguel Hernández University, where he is currently an Associate Professor with the Department of Materials Science, Optics and Electronic Technology. His current research interests include printed antennas, passive and active microwave devices, bioelectronics, and microwave imaging systems for tumor detection.

• • •